Pyrolysis of Kapton® in Air: An *in Situ* DRIFT Study

E. E. ORTELLI, F. GEIGER, T. LIPPERT,* and A. WOKAUN

General Energy Research, Paul Scherrer Institut, CH-5232 Villigen PSI, Switzerland (E.E.O., F.G., T.L., A.G.); and Department of Chemical Engineering and Industrial Chemistry, Swiss Federal Institute of Technology, ETH Zentrum, CH-8092 Zürich, Switzerland (E.E.O., A.W.)

Diffuse reflectance infrared Fourier transform (DRIFT) spectroscopy was used to study the pyrolysis of polyimide (Kapton®). The samples were prepared in a KBr matrix, which did not show pronounced interferences, such as increased emissivity, during the measurements. The pyrolysis of Kapton® reveals pronounced differences from laser-induced (UV) decomposition. The polyimide system decomposes thermally in distinct steps, i.e., first the imide ring, without elimination of the carbonyl groups, followed by the aromatic system and then the carbonyl groups. Several intermediates, such as nitriles and alkynes, are identified. The quantitative analysis of the spectra suggests that Kapton® decomposes in two steps, i.e., as a growing particle with shrinking core followed by a shrinking particle. The growing particle with shrinking core is the nonreacted polymer as core and a polyamic structure as the growing part, while the shrinking particle is the complete pyrolysis of the polymer. The activation energies for these two steps were determined. The reaction rate appears to be diffusion controlled at low temperatures and surface reaction controlled at higher temperatures.

Index Headings: **Diffuse reflectance infrared Fourier transform spectroscopy; DRIFT; Kapton®; Pyrolysis; Polyimide.**

INTRODUCTION

During the past three decades, since the commercialization of Kapton®† polyimide, an impressive variety of polyimides have been synthesized.[1,2] Polyimides possess outstanding key properties, such as thermooxidative stability,[3] high mechanical strength,[4] excellent electrical[5] and optical properties,[6,7] and superior chemical resistance.[8] Recently polyimides have also been applied as membranes for gas separation.[9,10] A promising industrial process is the ablation of polyimides by excimer laser,[11] which allows the material to be etched with micrometer-size precision.[12,13] At the present time laser ablation of polyimide is a routine part of microelectronics packaging[14,15] and the fabrication of nozzles for ink jet printer heads.[16] In addition, laser irradiation is being explored as a means of generating uniform thin polymer films, which may also prove to be useful in electronic packaging as well as in other applications such as polyimide film coating of various materials.[17] The mechanism of laser ablation is supposedly photothermal, with additional photochemical features,[18] but is still discussed controversially.[19]

Pyrolysis of polyimide is used for the preparation of carbon materials, i.e., high-quality graphite films. Complete pyrolysis and carbonization of polyimide foils has the advantage that the films are carbonized without any change in shape and that it is possible to convert the carbonized material into graphite.[20] Pyrolysis and thermolysis of polymers are usually studied by thermal analysis methods, such as thermogravimetry, thermomechanical analysis, differential thermal analysis (TGA), and differential scanning calorimetry. These methods can be used to characterize polymer bulk properties, but no information regarding specific chemical functionalities has been provided. Volatile decomposition products evolve during heating of polymeric samples, which can be identified by coupling a mass analyzer or IR spectroscopy instrument to the purge of the thermal analysis instruments. However, gas compositions do not provide information about changes in polymer structure and are not helpful at all when polymers undergo structural changes without evident volatile products. IR spectroscopy provides a substantial quantity of information about the molecular structures of materials. Unfortunately, IR transmission measurements are not suitable for studies of surface species, because the infrared beam passes through the entire sample. The absorption bands of the bulk material largely cover the bands of the surface species.

In contrast, diffuse reflectance infrared Fourier transform (DRIFT) spectroscopy allows one to monitor solid-state structural changes. It is specifically designed to study powder samples, and is well known for its high sensitivity. A wide variety of materials can be analyzed by using DRIFT spectroscopy. Some materials can be analyzed neat, without any sample preparation, but polymers have to be diluted normally by embedding them into a matrix.

The quantitative interpretation of diffuse reflectance spectra is based on the theory developed by Kubelka and Munk[21–23] and extended by Kortüm et al.[24–26] in terms of the scattering of light in samples diluted in nonabsorbing matrices. In the developed model, mathematical simplification is achieved by assuming that the sample is comprised of a single absorbing material contained in a nonabsorbing matrix. Typically, nonabsorbing compounds such as KCl, KBr, or diamond powders are employed as a diluent. The Kubelka–Munk model predicts a linearity with a zero y-intercept between concentration and IR absorption.

The aim of this work is to investigate the reaction scheme of the thermally induced decomposition of Kapton in air and compare it to UV laser-induced decomposition. This approach should help determine whether the laser-induced decomposition (ablation) of Kapton is comparable to pyrolysis. With the use of DRIFT spectroscopy, the changes in the concentration of different functional groups of the polymer are monitored during the thermal decomposition process. This information is used to develop a kinetic reaction scheme and to calculate kinetic parameters.

Received 2 October 2000; accepted 1 December 2000.

* Author to whom correspondence should be sent.

† Kapton is a trademark of Du Pont Corporation.

0003-7028/01/5504-0412$2.00/0

EXPERIMENTAL

The experimental setup consists of a gas dosing system and the DRIFT spectroscopy apparatus. The gas dosing system is equipped with four mass flow controllers (Bronkhorst), as described elsewhere.[27] DRIFT spectroscopy measurements were performed with a Bruker Equinox 55/S Fourier transform infrared (FT-IR) instrument equipped with a liquid nitrogen-cooled mercury cadmium telluride (MCT) detector. All the samples were analyzed in a diffuse reflectance unit (Specac). The temperature in the reaction chamber can be regulated within ±1 K.[27] Spectra were obtained from the accumulation of at least 1024 scans at a resolution of 4 cm^{-1}.

The applied polyimide is PMDA-ODA (Kapton HN) foil (Goodfellow). The Kapton foil was scraped with a scraping knife into small particles. The scrapes were mixed with KBr (Uvasol, Merck) in a volume ratio of Kapton/KBr = 1:10. For the pyrolysis experiments KBr was selected as the matrix, in contrast to the laser-induced decomposition experiments,[42] where SiC was used. KBr was chosen because the emissivity did not increase drastically, as in the case of SiC, where it interfered with the measurements.

The procedure for the experiments is as follows. About 0.03 g of the Kapton–KBr mixture was placed in the sample holder of the DRIFT cell and packed with a pressure of 1 MPa, as described elsewhere.[29,30] The sample was heated in an inert gas atmosphere to the desired temperature with a heating rate of 10 K min^{-1}. The spectrum of the Kapton–KBr mixture at a given temperature was collected and used as the background spectrum. The feed gas composition was then changed to the reaction feed gas. The total flow and composition of the reaction feed gas depend on the experiment. The applied total pressure of the feed gas was 1 bar. The sample was kept under these conditions for several hours, during which period spectra were recorded at different times. The following experiments were carried out.

1. Thermal decomposition in inert gas. The sample was heated to 841 K and flushed with 50 mL_N min^{-1} argon (quality 5.0, Sauerstoffwerk Lenzburg AG).
2. Thermal decomposition in air. The sample was heated in nitrogen (quality 5.0, Sauerstoffwerk Lenzburg AG) to the desired temperature; then the feed gas was changed to air (compressed air). The applied total flow was 50 mL_N min^{-1}. The experiment was carried out at several temperatures, i.e., 727, 755, 783, 794, 812, and 841 K.
3. Influence of the oxygen concentration on the pyrolysis. The sample was heated in nitrogen to the desired temperature; then the feed gas was changed to a mix consisting of 25% of compressed air and 75% nitrogen. The applied total flow was 50 mL_N min^{-1}. The experiment was repeated at 772 and 823 K.
4. Influence of the total flow on the thermal decomposition in air. The Kapton–KBr mixture was heated in nitrogen to 841 K; then the feed gas was changed to air. The applied total flow was 12.5 mL_N min^{-1}, which was only ¼ of the flow in the other experiments.

RESULTS AND DISCUSSION

Qualitative and Quantitative Analysis of the DRIFT Spectra. DRIFT spectra are usually presented in Kubelka–Munk units. DRIFT spectra with small baseline errors can be obtained when measurements are made at ambient temperature. However, if measurements are performed at higher temperatures, IR radiation emitted from the heated sample can affect the collected spectra, especially if MCT detectors are employed. This effect is even more pronounced when the refractivity of the sample changes with time. The baseline artifacts are added to the collected spectra.

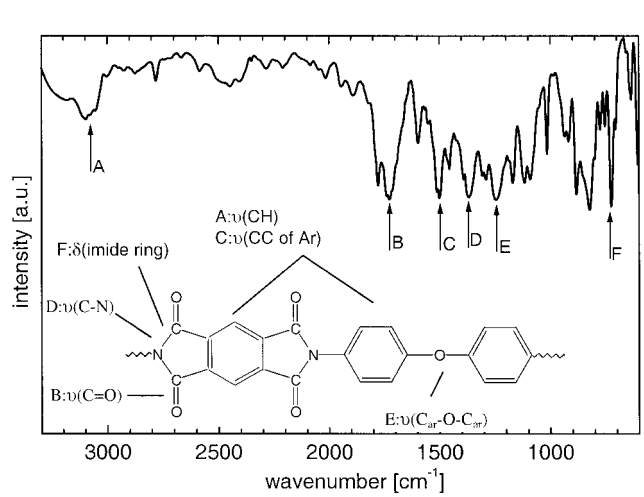

FIG. 1. DRIFT spectrum of Kapton; 1024 scans with a resolution of 4 cm^{-1} using KBr as the background and matrix. The following bands are assigned: (***A***) 3060 cm^{-1}: C–H stretching of hydrogen at the aromatic rings; (***B***) 1740 cm^{-1}: C=O stretching; (***C***) 1500 cm^{-1}: aromatic ring stretching; (***D***) 1390 cm^{-1}: C–N stretching of the imide rings; (***E***) 1260 cm^{-1}: C_{ar}–O–C_{ar} stretching of aryl ether; (***F***) 725 cm^{-1}: out-of-plane bending of the imide ring. The assigned vibrational bands are marked in the inserted molecular scheme.

To remove these artifacts, we used the procedure proposed by White.[31,32] Each collected spectrum was referred to a suitable background spectrum. The collected reflectance spectra were converted to apparent absorbance format, the baseline adjusted, and the spectra reconverted to reflectance. The corrected reflectance spectra were then used to evaluate the concentration of the desired compounds quantitatively. The use of relative reflectance units (I/I_0) to present the spectra is more appropriate, due to the change of reflectance of the sample during decomposition. An increase in surface species corresponds to an increase in absorption and therefore to negative peaks (going down) and peak areas. The peaks that are going up denote a decreasing band, due to the reduced absorption of disappearing species.

In Fig. 1, a spectrum of Kapton in KBr with KBr as background is shown. The broad band around 1740 cm^{-1} is due to the C=O stretching vibration (see band B). The sharp peak at 1600 cm^{-1} and the band at 1500 cm^{-1} (see band C) are assigned to the stretching vibration of both aromatic rings (1,2,4,5-tetrasubstituted and 1,4-disubstituted). The broad absorption at 1390 cm^{-1} (see band D in Fig. 1) and at 1250 cm^{-1} (see band E in Fig. 1) are assigned to the C–N stretching vibration in the imide ring and to the asymmetric C_{Ar}–O–C_{Ar} stretching vibration of the aryl ether, respectively. C_{Ar} indicates the carbon atom of the aromatic ring. The C–H in-plane bending vibrations of the aromatic rings are located between 1070 and 1015 cm^{-1}. The broad absorption around 880 cm^{-1} con-

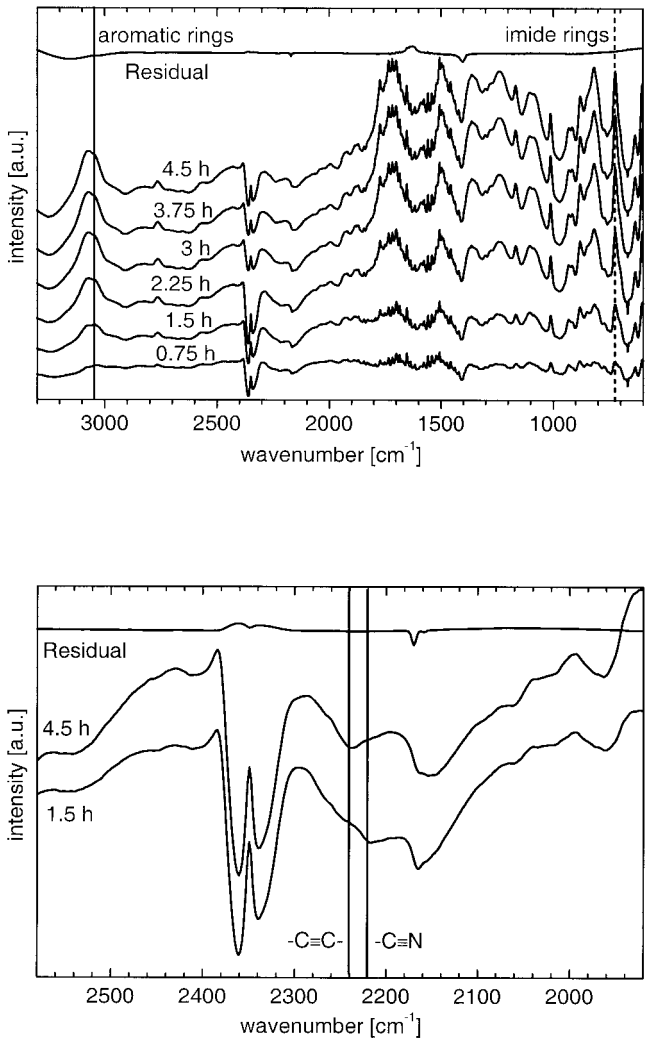

FIG. 2. (Top) DRIFT difference spectra of Kapton obtained with 1024 scans. The untreated KBr–Kapton mixture was used as the background. The sample was heated to 812 K in nitrogen and then kept at this temperature in air with a total flow of 50 mL_N min^{-1}. The spectrum marked as "Residual" was collected after completion of the reaction (15 h) and measured with KBr as the background. The marked bands correspond to the C_{ar}–H stretching vibration of the aromatic rings (3060 cm^{-1}) and to the out-of-plane bending vibration of the imide ring (725 cm^{-1}). (Bottom) Magnification of the 1920–2580 cm^{-1} region. The marked bands are the –C≡C– stretching (2240 cm^{-1}) and the –C≡N stretching (2220 cm^{-1}) vibration.

sists of several contributions; the most important are the C–H out-of-plane bending vibrations of aromatic rings. The sharp band at 725 cm^{-1} (see band F) is assigned to the out-of-plane bending vibration of the imide ring. At higher wavenumbers a broad absorption around 3060 cm^{-1} (see band A) is assigned to the C_{Ar}–H stretching vibrations of hydrogen located at the aromatic ring. An exhaustive investigation and discussion of the band assignments can be found in the literature.[33–45]

Thermal Decomposition in Inert Gas. An experiment was carried out to investigate the thermal decomposition of Kapton. The sample was heated to 841 K and kept at this temperature in argon. After 12 h only a small reduction of the Kapton bands was observed (data not shown), indicating that Kapton in a KBr matrix is stable up to this temperature. It was not possible to reach higher temperatures with the applied experimental setup. Therefore,

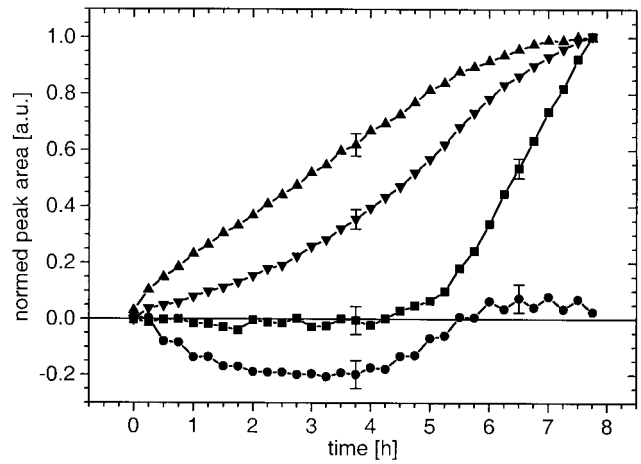

FIG. 3. Changes of the normalized peak area of the bands at 725 cm^{-1} [(▲) the out-of-plane bending of the imide ring], at 3060 cm^{-1} [(▼) C–H stretching vibrations of the aromatic ring], at 1750 cm^{-1} [(■) imide and amide C=O stretching vibration], and at 2220 cm^{-1} [(●) – C=N stretching vibration]. The experiment was performed at 812 K using a total flow of 50 mL_N min^{-1} of compressed air.

it was impossible to study the carbonization decomposition of Kapton in an inert gas atmosphere at very high temperatures.

Chandrasakhar and White[46] reported an influence of alkali halides on the thermal decomposition of polymers (PMMA and PHEMA). In the case of Kapton no influence of the KBr matrix on the decomposition process could be identified during TGA analysis (data not shown). This result is consistent with data reported in the literature about the resistivity of polyimides towards chemical agents. Concentrated H_2SO_4 or fuming HNO_3 is the only solvent.[47] Therefore, KBr can be applied as a matrix for the thermal decomposition experiments.

Thermal Decomposition in Air. In Fig. 2, DRIFT spectra of the pyrolysis of Kapton in air at 783 K are shown. These spectra are difference spectra, with Kapton in KBr as the background at the given temperature. In all further experiments the difference spectra were used. As expected, with increasing time, all bands are going up, indicating a continuous decomposition of the polymer. New bands are formed around 2220 cm^{-1} (see Fig. 2 bottom) and with increasing time at 2240 cm^{-1}. These groups are intermediates, which decompose completely at the end of the process, shown with ● in Fig. 3 and by the spectrum named "Residual" (see below) in Fig. 2. The high-frequency band can be assigned to the stretching vibration of alkynes (–C≡C–), while the band at 2220 cm^{-1} is assigned to the stretching vibration of conjugated nitriles (–C≡N). The red shift of its maximum, compared to reference data,[42] suggests that alkyne groups in central position (–C–C≡C–C–) might also be involved. Nitriles and alkynes were already identified as intermediates during the UV laser-induced decomposition of Kapton.[28] It is also noteworthy that most reference data are recorded at room temperature, while our spectra are recorded at high temperatures. It is well known that IR bands can shift with temperature changes. This shift is dependent on the vibrational mode; typically red shifts of 3 cm^{-1}/100 K are observed, but sometimes only broadening or even blue shifts are detected.[48,49,50] This effect is a man-

ifestation of the anharmonicity of a given vibrational band and the volume changes as a function of temperature. Therefore, it is quite difficult to assign new bands at elevated temperatures.

The spectrum (in Fig. 2) marked with "Residual" was collected at the end of the process (15 h), and pure KBr was used as the background. In this spectrum Kapton signals cannot be observed, suggesting a complete pyrolysis of the polymer. Noteworthy is the absence of carbon–carbon bands, indicating a total pyrolysis of the investigated compound. The band at 1640 cm^{-1} reveals a decrease in the water content, typically present in KBr. The two bands located at 2160 and 1400 cm^{-1} can be assigned to CO in a KBr matrix[51,52] and to cyano-groups bound to an aliphatic group ($–CH_2–CN$).[41] Black residue particles were observed optically after the pyrolysis experiments. These particles consist mainly of carbon, as suggested by energy-dispersive X-ray (EDX) analysis. This result proves that a weak carbonization process is also active.

The peak areas of all relevant bands were evaluated as a function of the time to analyze the kinetics of the pyrolysis process. In Fig. 3 the normalized changes of peak areas of several bands are shown for a temperature of 812 K. Four different behaviors can be identified. The bands assigned to the imide system (bands D and F in Fig. 1) decrease rapidly (see ▲ in Fig. 3; the out-of-plane bending vibration of the imide ring is shown). The bands related to the aromatic rings (A, C, and E in Fig. 1) reveal a two-step curve (see ▼ in Fig. 3), with an initial slow decomposition followed by a more rapid decomposition. The bands assigned to the carbonyl stretching vibration of the amide and imide (B in Fig. 1) groups, which are marked with ■ in Fig. 3, remain quasi-constant, until a fast decrease at the end of the pyrolysis. The curve marked with ● represents an intermediate, i.e., the $–C{\equiv}N$ stretching band at 2220 cm^{-1}, which decomposes again completely. The alkynes ($–C{\equiv}C–$) show the same behavior as the nitrile band. It is noteworthy that the carbonyl bands of the amide and imide decrease only at a very late stage of the pyrolysis, when the intermediates are already more or less decomposed.

The weak presence of bands in the region of the aliphatic C–H stretching vibrations (2980–2780 cm^{-1}) indicates that only a very small number of aliphatic structures are formed. This observation is also consistent with the band at 1400 cm^{-1} that was assigned to a $–CH_2–CN$ group.

Figure 3 shows (▲, ▼, and ■) that different structural parts of Kapton decompose at different times. Intermediates are formed at the same time (● in Fig. 3) and subsequently pyrolyzed again. This pattern suggests that Kapton decomposes completely in air via a multi-step process, without the formation of polymers with low molecular weight.

The bands representing the out-of-plane bending vibrations of the imide ring (see the band at 725 cm^{-1} in Fig. 2) and the C–H stretching vibrations of the aromatic rings (see the band at 3060 cm^{-1} in Fig. 2) were examined in more detail for a quantitative analysis. These two bands were chosen because they are directly related to a specific part of the polymer and they are at an isolated position in the IR spectrum, avoiding the interference of

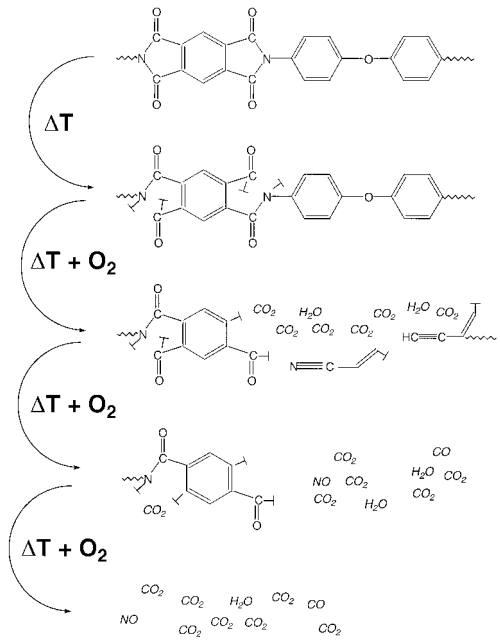

FIG. 4. Suggested scheme of the thermal decomposition of Kapton, including various intermediates, assuming a total oxidation of the carbon. ⊥ indicates a broken bond; information on the nature (radicalic, ionic, terminated) is not available from the present experiments.

neighboring bands. In other regions of the IR spectrum the qualitative and quantitative analysis is very difficult due to the complex band structure in the region where, e.g., C–C (1260–800 cm^{-1}), C=C (1680–1620 cm^{-1}), C–O (1270–1060 cm^{-1}), C=O (1800–1700 cm^{-1}), and C–N (1420–1400 cm^{-1}) groups absorb.

The C–N bonds of the imide rings were identified as primary decomposition sites during the pyrolysis of Kapton. The resulting structures can be described best as amide groups. The next step is the decomposition of the aromatic systems. Simultaneously, $–C{\equiv}N$ and $–C{\equiv}C–$ groups are formed as intermediates. The last step of the decomposition is the elimination of the carbonyl groups. A carbon- and nitrogen-rich residue remains.

A scheme suggesting a possible decomposition mechanism is shown in Fig. 4. This scheme includes the detected intermediates and assumes a total oxidation of the carbon. It is difficult to quantify the oxidation product, CO_2, in the DRIfT spectra, because it is a trace impurity in the feed gas. A clear difference between pyrolysis and UV laser (308 nm)-induced decomposition of Kapton is detected. During laser-induced decomposition, the diaryl ether group decomposes simultaneously with the imide system, while the decomposition of the ether bridge is not clearly observed during pyrolysis. The decomposition of the imide system during photolysis results in the formation of amide systems which decompose again quite fast under elimination of the carbonyl groups, which is one of the last steps of decomposition during pyrolysis. In both cases—i.e., photolysis and pyrolysis—the formation of aliphatic hydrocarbons, nitriles, and alkynes is observed, but isocyanate groups are observed only during photolysis. These results clearly show that the mechanism of UV laser-induced decomposition is not identical to pyrolysis, as suggested previously.[18]

Modeling of Time Dependence. *Simple Topological*

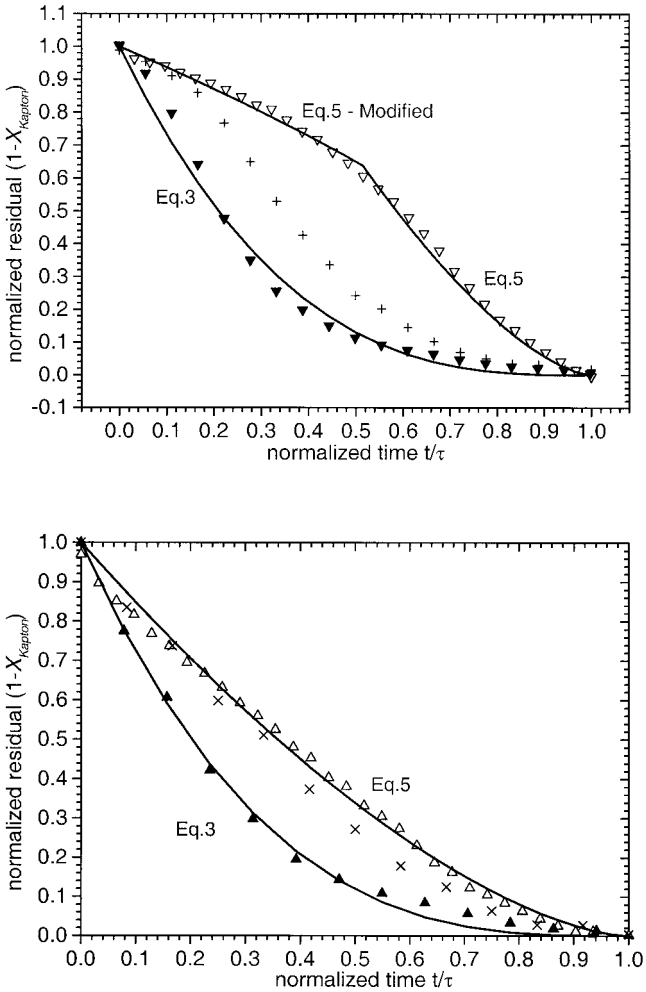

FIG. 5. Normalized residual ($1 - X_{Kapton}$) as function of the normalized time for a complete conversion (t/τ) at 783 K (open symbols), 812 K (+ and ×), and 841 K (solid symbols). The equations applied for fitting the data points are included in the plot (see text). (Top) The band at 3060 cm^{-1} (▼, ▽, and +) representing the aromatic rings. (Bottom) The band at 725 cm^{-1} (▲, △, and ×), representing the imide rings.

Description of the Overall Reaction. A better understanding of the reaction can be achieved by plotting the conversion of a specific structural unit. The conversion is proportional to the normalized peak area and is plotted vs. the normalized time necessary for the complete reaction.[21–26] Similar plots are used in heterogeneous catalysis to study the rate-controlling step of a process.[53] In Fig. 5, top, a plot for the aromatic rings (3060 cm^{-1}) at temperatures of 783 K (▽), 812 K (+), and 841 K (▼) is presented. In Fig. 5, bottom, the imide system (725 cm^{-1}) is plotted at the same temperatures [783 K (△); 812 K (×); and 841 K (▲)].

High Temperatures—Reaction Control. At the highest applied temperature (841 K: solid symbols in Fig. 5) the plots decrease rapidly to ≈20% of the initial concentration, followed by a slow decrease to zero. This evolution is typical for a chemical reaction control process. The rate velocity of such a process can be described by Eq. 1.[53]

$$S_{ex}^{-1}\frac{dN_{Kapton}}{dt} = -k_s C_{O_2} \quad (1)$$

The sample is represented by a constant number of similar particles. S_{ex} is the external surface of the particle, which can be approximately described as a sphere ($S_{ex} = 4\pi r^2$). N_{Kapton} is the mole number of Kapton, C_{O_2} is the molar concentration of oxygen in the gas flow, and k_s is the reaction velocity on the surface of the particle. By solving Eq. 1, one obtains the time t necessary to oxidize a particle as a function of the radius (R_0 and R_t) of the particle (Eq. 2).

$$t = \frac{\rho_{Kapton}}{k_s C_{O_2}}(R_0 - R_t) \quad (2)$$

ρ_{Kapton} is the molar density of Kapton. R_0 is the radius of the starting particles, while R_t denotes the radius of the particles at the time t. The time τ required for complete conversion is given for $R_t = 0$. The decrease in the radius, or increase in fractional conversion of the particle X_{Kapton} as a function of the normalized time (t/τ), is given in Eq. 3.

$$\left(\frac{R_t}{R_0}\right)^3 = 1 - X_{Kapton} = \left(1 - \frac{t}{\tau}\right)^3 \quad (3)$$

For the exponent in Eq. 3, a variable is used to fit the data points for the aromatic and imide system in Fig. 5. At the highest temperature (solid symbols), a value of 3.0 ± 0.1 is obtained for exponent. This shows that this step is a chemical reaction control process.

Low Temperatures—Shrinking Particle. At the lower temperature (783 K: open symbols in Fig. 5), substantially different behavior is observed. The imide band (△ in Fig. 5, bottom) decreases quasi-linearly with the elapsed time (see Equation 5). The aromatic band (▽ in Fig. 5, top) is complex, revealing two distinct decomposition patterns. At the beginning (first half) of the normalized time, a slow linear decrease is observed, followed by a fast decrease. The decrease in the imide band and the change in the aromatic band in the second part of the curve are typical for a film diffusion control reaction of shrinking particles in a gas flow in the Stokes regime. To confirm this observation, we used a new mathematical model to fit the curves.[53] Starting from Eq. 1, the reaction velocity k_s is substituted with $k_g = DR_t^{-1}$.[53] D is the diffusion velocity, and k_g the mass transfer coefficient between fluid and particle. The differential equation is solved, and the time necessary to reduce a particle from a starting radius R_0 to R_t is obtained (see Eq. 4).[53]

$$t = \frac{\rho_{Kapton} R_0}{2DC_{O_2}}\left(1 - \left(\frac{R_t}{R_0}\right)^2\right) \quad (4)$$

The fractional conversion of the particle X_{Kapton} as a function of the normalized time (t/τ) is shown in Eq. 5.

$$1 - X_{Kapton} = \left(1 - \frac{t}{\tau}\right)^{3/2} \quad (5)$$

The data points (open symbols) in Fig. 5 were fitted by using Eq. 5 with the exponent as a variable. The obtained values, around 1.5 ± 0.1, confirm the hypothesis of the film diffusion control reaction of shrinking particles in the Stokes regime.

Refinement at Low Temperature—Differences Imide/Aromatics. The aromatic band (▽ in Fig. 5, top) decreases slowly and linearly in the first part of the plot. Fitting of this part of the data, considering a shrinking particle,

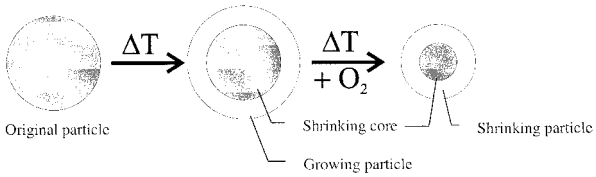

FIG. 6. Suggested decomposition scheme: shrinking particle with a shrinking core. The pyrolysis of the core has an Arrhenius activation energy of E_A = 162 ± 19 kJ mol^{-1} (imide rings), and the pyrolysis of the residual particle one of E_A 212 ± 37 kJ mol^{-1} (aromatic rings).

did not give satisfactory results. The first part of the plot (open symbols in Fig. 5, top) is fitted by using Eq. 5, with the exponent as a variable. The obtained value of $n \approx 0.6$ suggests that the model for Eq. 5 is not really valid in this case. A mathematical analysis of the exponent in Eq. 5 reveals that this value is dependent of the particle radius (see Eq. 6). The left side in Eq. 5 is substituted by a volume ratio of the particles at the start (R_0') and a given time (R_t). The exponent on the right side is substituted with the variable x.

$$\left(\frac{R_t}{R_0'}\right)^3 = \left(1 - \frac{t}{\tau}\right)^x \tag{6}$$

Equalizing $(1 - t/\tau)$ from Eqs. 5 and 6 and solving for the volume ratio yields a relation between the actual starting radius R_0' (Eq. 6) and the theoretical starting radius of R_0 (as in Eq. 5).

$$\left[\left(\frac{R_t}{R_0'}\right)^3\right]^{1/x} = \left[\left(\frac{R_t}{R_0}\right)^3\right]^{2/3} \tag{7}$$

Solving Eq. 7 for R_0 gives the relation

$$R_0 = (R_t^{2x-3} R_0'^3)^{1/2x} \tag{8}$$

The analysis of Eq. 8 shows that, for values of $x < 1.5$, the theoretical radius R_0 is larger than the actual starting radius R_0'. This observation implies that the particles expand temporarily, followed by shrinking. A tentative representation of the decomposition mechanism is shown in Fig. 6. An increase in the polymer surface is a well-known effect during polymer decomposition.[54] An accumulation of gaseous products will also result in surface swelling.[55] This observation is consistent with an immediate decomposition of the imide ring, causing an increase in the surface area of the particle, and the delayed decomposition of the aromatic rings. This behavior explains the unsatisfactory results obtained for other decomposition mechanism models (see above) and the observation of a multi-step process for the pyrolysis of Kapton.

Estimation of Activation Energies of Consecutive Steps. The activation energies for the two distinct processes visible in Figs. 3 and 5 were extracted to obtain quantitative kinetic data on the thermal decomposition of Kapton. For this purpose, reaction rate constants are calculated for the imide signal (first step in Fig. 6) and from the aromatic signal at high turnovers (second step in Fig. 6). The reaction rate constants were calculated (in Fig. 3) with the assumption that the pyrolysis process starts as a first-order reaction. In the case of the imide system, a linear regression of the short-time turnover with zero x/y intercept (initial rate) is used for the analysis. For the

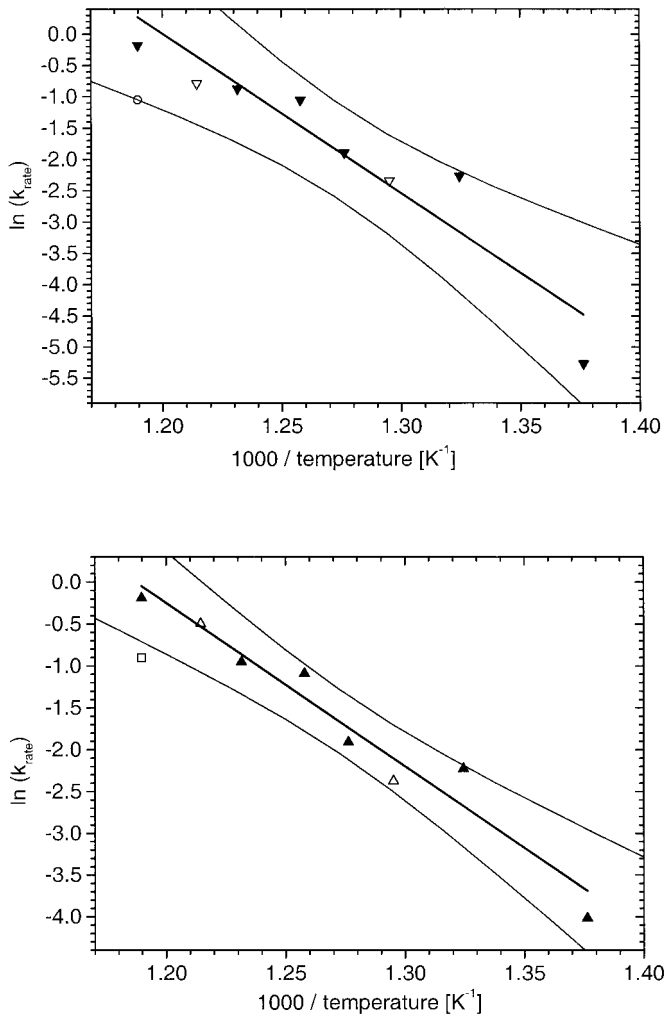

FIG. 7. Arrhenius plots and confidence range (2σ) for the decomposition of the aromatic systems (top) and imide rings (bottom). Only solid symbols (▼ and ▲) are used for the calculation of the Arrhenius activation energies. (Top) Band at 3080 cm^{-1} for the following conditions: 50 mL$_N$ min^{-1} air (▼); 12.5 mL$_N$ min^{-1} air and 37.5 mL$_N$ min^{-1} N_2 (▽); and 12.5 mL$_N$ min^{-1} (○). (Bottom) Band at 725 cm^{-1} for the following conditions: 50 mL$_N$ min^{-1} air (▲); 12.5 mL$_N$ min^{-1} air and 37.5 mL$_N$ min^{-1} N_2 (△); and 12.5 mL$_N$ min^{-1} air (□).

aromatic ring the slope at $t \geq 4.5$ h in Fig. 3 is used to calculate the reaction rate. This value corresponds to the faster second reaction step visible in Fig. 5 (top), corresponding to the second step in Fig. 6 (shrinking particle). This reaction step reaches the maximum velocity only after an incubation period. Therefore, a linear regression without zero x/y intercept is used. The Arrhenius plot for the decomposition of the imide rings (▲ in Fig. 7, bottom) and of the aromatic ring (▼ in Fig. 7, top) is shown in Fig. 7. From this plot the Arrhenius activation energy E_A is calculated according to Eq. 9.

$$\ln k = \ln A - \frac{E_A}{R} T^{-1} \tag{9}$$

The obtained values are E_A (imide rings, early time) = 162 ± 19 kJ mol^{-1}, and E_A (aromatic ring decomposition, late phase) = 212 ± 37 kJ mol^{-1}. This result is consistent with the observation of a rapid decomposition of the imide rings, followed by the decomposition of the aromatic systems. The obtained values agree quite well with values

reported in the literature. Traeger and Salazar[56] reported an activation energy of 163 ± 20 kJ mol^{-1} for the pyrolysis of Kapton in air, while Heacock and Berr[57] published values between 162 and 165 kJ mol^{-1}. The same authors reported a two-step process with an activation energy of 232 kJ mol^{-1} for the thermal degradation of polyimide in helium. All these experiments were performed at temperatures between 523 and 723 K with the use of TGA. This result confirms that DRIFT spectroscopy can be used to analyze *simultaneously* the decomposition mechanism *and* kinetics of polymers (at least Kapton).

Reflections on Refined Topological Models. As there are at least two reactions, the actual situation would correspond to a shrinking core (undecomposed polymer) with an initial expansion rather than a shrinking shell of aromatics. To analyze the rate constants and activation energies for this situation, we would need to develop a new mathematical model and to perform the experiments at low temperatures where this behavior could be observed. Additionally, another quite plausible model, i.e., an ash diffusion reaction control model, was tested (see Eq. 10)[53] for the imide pyrolysis.

$$\left(1 - \frac{t}{\tau}\right) = 3(1 - X_{\text{Kapton}})^{2/3} - 2(1 - X_{\text{Kapton}}) \quad (10)$$

No satisfactory results were obtained with this model. This is probably due to the fact that this model is not really valid for shrinking particles.[53] The ash diffusion model was also applied for the high-temperature experiments. The model agrees quite well with the experimental data at the end of the reaction, where the accumulation of carbon species might play a role. This approach is also in agreement with the EDX data and optical detection of small amounts of carbon materials after the pyrolysis (data not shown).

Influence of the Oxygen Concentration. The O_2 concentration in the feed gas was reduced to 25% of the concentration in air. The experiment was repeated at two different temperatures, i.e., 772 and 823 K. The changes in the concentration of the different functional groups are very similar (data not shown) to those obtained in air. The reaction rate was calculated as described previously. The obtained values are included in the Arrhenius plots [Fig. 7: aromatic rings (▽ in upper graph) and imide rings (△ in the lower graph)]. The calculated parameters are close to the fit, indicating that the reaction rate constants are not influenced by the applied O_2 concentration in the gas phase (at least within the tested range). This result suggests that the process is, depending on the applied temperature and gas flow, controlled by either the chemical reaction or the product desorption/diffusion.

Influence of the Total Flow. A simple test to assess the influence of the total gas flow was carried out. The feed gas of compressed air was reduced to 12.5 mL_N min^{-1}, which is only a quarter of the flow in the previous experiments. The experiment was performed only at the highest temperature (841 K). The change in the concentrations assigned to the different functional groups differs from those obtained with the higher flow and lies between the data obtained at 783 and 812 K (data not shown). The reaction rate was calculated as described above. The obtained values are included in the Arrhenius plots [Fig. 7: aromatic rings (○ in the upper graph) and imide rings (□ in the lower graph)]. The calculated values are consistently below the values obtained in the previous experiments, indicating a reduced reaction rate velocity. This result might be due to a reduction in the overall diffusion, caused by the increased thickness of the gas film.

The same variation in the rate constant can be obtained by changing the temperature. A relatively small increase in the temperature is equivalent to a large increase in the gas flow, probably significantly reducing the film diffusion resistance. This result is consistent with the previously described observations of a film diffusion control process at low temperatures and a chemical reaction control at high temperatures.

CONCLUSION

The experimental data show that KBr can be used for pyrolysis experiments of Kapton by DRIFT spectroscopy. No artifacts are observed with and without the sample upon heating to 841 K. The spectra (i.e., difference spectra) are obtained rapidly, the position of a given band is related to a specific functional group, and the peak area can be used for quantitative analysis. The pyrolysis of Kapton shows pronounced differences from laser-induced (UV) decomposition. The polyimide system decomposes thermally in distinct steps—i.e., first the imide ring, without elimination of the carbonyl groups, followed by the aromatic system and then the carbonyl groups. Several intermediates, such as nitriles and alkynes, are identified. The quantitative analysis of the spectra suggests that Kapton decomposes in two steps, i.e., as a growing particle with shrinking core followed by a shrinking particle. The growing particle with a shrinking core is the nonreacted polymer as the core and a polyamic structure as the growing part, while the shrinking particle is the complete pyrolysis of the polymer. The activation energies for these two steps are 162 ± 19 and 212 ± 37 kJ mol^{-1}, respectively. The reaction rate appears to be diffusion controlled at low temperatures and surface reaction controlled at higher temperatures. The oxygen concentration has no pronounced influence within the tested range. DRIFT spectroscopy has potential as an important analytical tool for the decomposition of polymers. Information on the mechanism, thermal properties, and kinetic data can be obtained simultaneously.

ACKNOWLEDGMENT

The authors are grateful to Dr. M. Meli for suggestions on the manuscript.

1. C. E. Sroog, in *Polyimides: Fundamental and Applications,* M. K. Gosh and K. L. Mittal, Eds. (Marcel Dekker, New York, 1996), p. 1.
2. C. D. Dimitrakopoulos, E. S. Machlin, and S. P. Kowalczyk, Macromolecules **29,** 5818 (1996).
3. T. Matsumoto, Macromolecules **32,** 4933 (1999).
4. M. Hasegawa, N. Sensui, Y. Shindo, and R. Yokota, Macromolecules **32,** 387 (1999).
5. Y. T. Chern, Macromolecules **31,** 5837 (1998).
6. S. M. Pyo, S. I. Kim, T. J. Shin, H. K. Park, M. Ree, K. H. Park, and J. S. Kang, Macromolecules **31,** 4777 (1998).

7. J. P. Chen, F. L. Labarthet, A. Natansohn, and P. Rochon, Macromolecules **32,** 8579 (1999).
8. A. Wilson, in *Polyimides,* K. L. Mittal, Ed. (Plenum, New York, 1984), p. 715.
9. H. Kawakami, M. Mikawa, and S. Nagaoka, Macromolecules **31,** 6636 (1998).
10. M. R. Coleman and W. J. Koros, Macromolecules **32,** 3106 (1999).
11. H. Brannon, J. R. Lankard, A. L. Baise, F. Burns, and J. Kaufman, J. Appl. Phys. **58,** 2036 (1985).
12. E. Andrew, P. E. Dyer, D. Forster, and P. E. Key, Appl. Phys. Lett. **43,** 717 (1983).
13. R. Srinivasan and B. Braren, J. Polym. Sci. **22,** 2601 (1984).
14. F. Bachman, Chemtronics **4,** 149 (1989).
15. J. R. Lankard and G. Wolbold, Appl. Phys. A **54,** 355 (1992).
16. See, for example, H. Aoki, U.S. Patent 5736999 (1998)
17. S. G. Hansen and T. E. Robitaille, Appl. Phys. Lett. **52,** 81 (1988).
18. S. Küper, J. Brannon, and K. Brannon, Appl. Phys. A **56,** 43 (1993).
19. R. Srinivasan, Appl. Phys. A **56,** 417 (1993).
20. M. Inagaki, T. Takichi, Y. Hishiyama, and A. Obslei, in *Chemistry and Physics of Carbon,* P. A. Thrower and L. R. Radovic, Eds. (Marcel Dekker, New York, 1999), Chap. 3.
21. P. Kubelka and F. Munk, Z. Tech. Phys. **12,** 593 (1931).
22. P. Kubelka, J. Opt. Soc. Am. **38,** 1067 (1948).
23. P. Kubelka, J. Opt. Soc. Am. **44,** 330 (1954).
24. G. Kortüm, Spectrochim. Acta **6,** 534 (1957).
25. G. Kortüm, Trans. Faraday Soc. **58,** 1624 (1962).
26. G. Kortüm, W. Braun, and G. Herzog, Angew. Chem. Intern. Ed. **2,** 333 (1963).
27. E. E. Ortelli and A. Wokaun, Vib. Spectrosc. **19,** 451 (1999).
28. E. E. Ortelli, F. Geiger, T. Lippert, J. Wei, and A. Wokaun, Macromolecules **33,** 5090 (2000).
29. S. A. Yeboah, S.-H. Wang, and P. R. Griffths, Appl. Spectrosc. **38,** 259 (1984).
30. J. M. Weigel, C. Fröhlich, A. Baiker, and A. Wokaun, Appl. Catal. **140,** 29 (1996).
31. R. L. White, Appl. Spectrosc. **46,** 1508 (1992).
32. R. L. White, Anal. Chem. **64,** 2010 (1992).
33. R. W. Snyder, C. Wade Sheen, and P. C. Painter, Appl. Spectrosc. **42,** 503 (1988).
34. G. F. L. Ehlers, K. R. Fisch, and W. R. Powell, J. Polym. Sci. **8,** 3511 (1970).
35. H. Ishida, S. T. Wellinghoff, E. Baer, and J. L. Koenig, Macromolecules **13,** 826 (1980).
36. T. Sakuma, S. Ogitani, and A. Ikeda, J. Photopolym. Sci. Technol. **8,** 277 (1995).
37. M. C. Buncick and D. D. Denton, J. Vacuum Sci. Technol. **A9,** 350 (1991).
38. R. W. Snyder and C. W. Sheen, Appl. Spectrosc.**42,** 296 (1988).
39. C. Digiulio, M. Gautier, and B. Jasse, J. Appl. Polym. Sci. **29,** 1771 (1984).
40. G. W. Mayer, T. E. Glass, H. J. Grubbs, and J. E. McGrath, Polym. Prepr. **35,** 549 (1994).
41. M. J. Brekner and C. Geger, J. Polym. Sci. **25(A),** 2005 (1987).
42. G. Socrates, in *Infrared Characteristic Group Frequencies* (John Wiley and Sons, New York, 1994).
43. N. A. Borisevich and N. N. Khovratovich, Opt. Spectrosc. **10,** 309 (1961).
44. S. Molis, in *Proceedings of Third International Conference on Polyimides,* Ellenville, New York (1988), p. 87.
45. J. S. V. Deshpande, E. Gulari, J. Kanicki, and W. L. Warren, J. Appl. Phys. **80,** 5028 (1996).
46. T. M. Chandrasekhar and R. L. White, J. Appl. Polym. Sci. **60,** 1209 (1996).
47. C. E. Sroog, A. L. Endrey, S. V. Abramo, C. E. Berr, W. M. Edwards, and K. L. Olivier, J. Polym. Sci. **A-3,** 1373 (1965).
48. P. Gillet, F. Guyot, and J. M. Malezieux, Phys. Earth and Planetary Interiors **58,** 141 (1989).
49. O. L. Anderson and J. Susuki, J. Geophys. Res. **88,** 3549 (1983).
50. T. Lippert and P. O. Stoutland, Appl. Surf. Sci. **109/110,** 43 (1997).
51. J. B. Peri, J. Phys. Chem. **72,** 2917 (1968).
52. J. B. Peri, J. Phys. Chem. **86,** 1615 (1982).
53. O. Levenspiel, *Chemical Reaction Engineering* (John Wiley and Sons, New York, 1972), Chap. 12.
54. H. G. Elias, *Makromoluküle* (Hütig and Wepf Verlag, Basel, Heidelberg, 1975).
55. T. Lippert, R. L. Webb, S. C. Langford, and J. T. Dickinson, J. Appl. Phys. **85,** 1838 (1999).
56. R. K. Traeger and E. A. Salazar, Polym. Preprints **12,** 292 (1971).
57. J. F. Heacock and C. E. Berr, SPE Trans. **5,** 105 (1965).